Proceedings of the
Annual Stability Conference
Structural Stability Research Council
Atlanta, Georgia, April 21-24, 2020

Stability of composite axial members under fire loading

Preshit Wazalwar[1], Saahastranshu R. Bhardwaj[2], Ataollah Taghipour Anvari[3], Amit H. Varma[4]

Abstract
Composite axial members [Concrete-filled Steel Tube (CFT) columns and Composite-Plate Shear Walls (CPSWs)] may be subjected to a combination of loading conditions, such as gravity, wind, seismic or fire. Under fire loading, the member would experience degradation of material properties and non-uniform temperature distribution through the cross-section. A time-temperature study is necessary to determine the member capacity and stability under fire loading. A fiber-based numerical analysis tool was developed to model composite axial members. The fiber model was benchmarked using experimental results and further validated with benchmarked Finite Element (FE) models. The developed fiber-model can be used as a tool for the performance-based design of CFTs. A parametric study was conducted on CFTs using the developed fiber model. The study involved simulating fire conditions by exposing steel faceplates to elevated temperatures (ASTM E119 Time-Temperature Curve) while maintaining a constant axial load. The effect of various parameters such as column slenderness, column aspect ratio, section slenderness, and material properties on the behavior of the members at elevated temperatures was studied. It was observed that section slenderness and concrete strength have a significant effect on column capacity, while aspect ratio and steel yield strength have a minor influence. The parametric study results are used to develop equations for calculating the compression strength of CFTs at elevated temperatures.

1. Introduction

Concrete Filled Steel Tube (CFT) columns are composite members comprising rectangular or circular hollow structural sections (HSS or steel tubes) filled with concrete. These composite columns are popular in construction as they combine the structural properties and advantages of steel and concrete. The steel tube acts as formwork and primary reinforcement, and provides confinement to the concrete infill. The steel tube can improve the performance of concrete and cut down the need to erect and demolish separate formwork. The concrete infill acts as lateral support to the steel tube, delaying the local buckling of the steel tubes.

In the case of a fire event, a structural column may be exposed to uniform or non-uniform fire loading. The elevated temperatures cause degradation of the strength and stiffness of the material. A column carrying a constant axial load can fail when exposed to sustained heating. CFT columns typically have a better fire resistance compared to conventional steel columns. This is because a

[1] Graduate Research Assistant, Purdue University <pwazalwa@purdue.edu>
[2] Assistant Professor, The University of Alabama <saahas.bhardwaj@ua.edu>
[3] Graduate Research Assistant, Purdue University <ataghipo@purdue.edu>
[4] Karl H. Kettelhut Professor and Director of Bowen Laboratory, Purdue University <ahvarma@purdue.edu>

temperature gradient across the section of CFTs is developed at elevated temperatures. This temperature gradient is a result of the low thermal conductivity of concrete and results in lower temperatures within the concrete infill than steel. Hence, the concrete infill resists most of the applied axial load under fire loading and delays member failure.

Experimental studies of composite CFT columns using standard fire curves have been carried out and empirical equations have been proposed to predict their fire rating and capacity (Kodur and Mackinnon, 2000; Lie et al., 1995). Numerical studies conducted on CFTs have focused on understanding their fundamental behavior under fire loading, development and benchmarking of finite-element models. These finite element models, although accurate, are computationally expensive and cumbersome to run. The equations proposed in literature are primarily empirical, i.e. based only on the experimental results obtained by the researchers. They cannot be extended to generalized fire scenarios or structural designs other than those that were tested. These limitations result in a prescriptive design approach of composite structures under fire loading, thus limiting innovation and optimization.

There is a need for performance-based design methodologies for composite members which would allow a more diverse range of structures to be designed using composites. Additionally, there is a need for simplistic analytical models based on fundamental principles of mechanics that can predict the behavior of a broad category of composite structures under standard as well as user-defined fire loading scenarios. These tools will further aid in performance-based design of composite structures and permit a greater scope for optimization and innovation.

The current study analyzes the effect of structural and material parameters on the behavior and stability of composite axial members at elevated temperatures. A fiber-based 2D cross-section analysis model was developed to carry out the analyses. This model was benchmarked using experimental and Finite Element (FE) analysis. The development and benchmarking of this model for fire loading is summarized in the current paper. The developed fiber model was used to conduct a parametric study on CFTs considering various parameters. The results of the parametric study were utilized to develop a design equation to predict the axial compression strength of CFTs at elevated temperatures.

2. Background

Extensive studies have been conducted to evaluate the ambient behavior of composite members, under various combinations of axial, bi-axial and seismic loading. Numerical models to analyze composite members have been developed (Bhardwaj et al. 2019a). However, these models cannot be extrapolated to elevated temperatures because of: (i) temperature-dependent degradation of material properties at high temperatures and (ii) temperature gradient across the CFT section.

Several experimental studies have been conducted by researchers on composite members at elevated temperatures. These studies involved fire tests of CFT specimens in furnaces. The gas temperature was controlled to follow a standard time-temperature curve in the furnaces. A constant or varying axial or lateral load was applied. These studies mainly focused on material properties and fire resistance rating of the specimens. Lie et al. (1995) tested three specimens of hollow structural steel filled with bar-reinforced concrete. Material models for steel and concrete at elevated temperatures were developed based on the test results. An analytical approach was also proposed to calculate the axial capacity of reinforced square CFT members under uniform fire

conditions. Poh (2001) proposed a stress-strain-temperature relationship for structural steel based on experimental data. Kodur and Mackinnon (2000) used data from 58 tests on plain, bar-reinforced and fiber-reinforced CFTs to develop empirical equations for prediction of fire resistance ratings. These experimental studies focused on simulating fire scenarios as specified by the design codes, thus the empirical equations developed are applicable only to limited design cases.

Hong et al. (2008) developed FE model using ABAQUS (Simulia, 2016) to study the behavior of CFTs under fire loading. The models were benchmarked based on experimental data. The models were used to predict CFT response at elevated temperatures. Detailed development and benchmarking of these models is reported in Hong et al. (2008) and Hong (2007). FE models typically have a high level of detail and thus are computationally expensive. As a result, it may be difficult to use them in conventional design scenarios.

2D fiber-based models of CFTs have also been developed by Hong et al. (2009), which are simplified and computationally economical. Detailed development and validation of the model is reported in Hong (2007) and Hong et al. (2009). This model was found to be reasonably accurate in predicting key parameters of CFT behavior when compared to experimental data and FE analysis. 2D fiber-based models have the advantage of being simplified, requiring shorter run times. However, the 2D model developed by Hong et al. (2009) has a limited applicability (only applicable to square CFTs with uniform faceplate thickness and all-sided fires).

3. 2D Numerical Model

A 2D fiber-based numerical model to simulate composite axial members under fire loading was developed in the current study. The goal was to develop a quick and accurate tool for the design and analysis of composite axial members under fire loading. General-purpose computing software (MathWorks, 2019)was used as the platform to develop this model. The basic functionality of this fiber model was based on the fiber model developed by Hong (2007) and Hong et al. (2009). The model was designed to be applicable to a wide range of applications, which include CFTs, composite walls (CPSWs) and various fire scenarios (all-sided vs one-sided fires). Validation of the model was done by comparing the results with experimental data and FE analysis. The development and benchmarking process of the fiber model are presented in this section.

The 2D fiber-model is a fundamental section-based model which involves modeling a cross-section of the axial member. This cross-section is divided into discrete fibers consisting of nodes and elements. Incremental analysis is utilized, wherein the column is analyzed in its present state at each time step, and the analysis results are used to update the column state for the next time step. Every time step consists of three different analysis steps which are (a) 2D heat transfer analysis, (b) section moment-curvature analysis, and (c) non-linear column buckling analysis.

In the first step (2D heat transfer analysis), the temperature of each node and element of the section is calculated based on applied thermal material properties. Multiple time-temperature curves are programmed into the model to provide the flexibility of analysis. Also, the user can choose to directly specify the surface temperature or specify gas temperatures to calculate the surface temperature considering convection and radiation. The next step of the analysis involves generating a cross-section moment-curvature plot for the applied axial load and the calculated temperatures in the heat transfer analysis. The section moment for each curvature value is

calculated using an iterative process. An initial centroidal strain is assumed and its value is adjusted based on section equilibrium (i.e. summation of element forces equals the applied axial load). The net moment of the section is calculated by summing up the moment contribution of each element. The last step (non-linear column buckling analysis) utilizes a modified version of Newmark's method of inelastic column buckling analysis to simulate the overall column behavior. Newmark's method is modified to be applicable for elevated temperatures by using the moment-curvature plots generated in step 2. Iterations are carried out until a converged deflected shape is obtained which satisfies all equilibrium equations. Further details of these steps, equations and flowcharts are reported by Hong et al. (2009) and Hong (2007). The model checks for two modes of failure of the column, which are global buckling (instability) and yielding/crushing. The column is considered to have failed due to global instability when the maximum moment along the column length (typically at mid-span) exceeds the maximum moment that can be developed in the section (maximum moment in M-ϕ curve). The column is considered to fail in yielding if axial force equilibrium cannot be established at any step while generating the moment-curvature plot. This failure mode governs for short columns whereas longer columns typically undergo global instability failure.

Material Stress-strain-temperature Models

Multiple material models were programmed in the fiber model which allows the user to select the desired material model. Material models developed by Poh (2001) and Lie and Irwin (1995) have been programmed for steel. Also, the effective stress-strain model for steel developed by Lai et al. (2016) was utilized. This model was modified to work for elevated temperatures. To model concrete, the model developed by Lie (1992) has been utilized. Stress-strain-temperature curves for steel and concrete proposed in Eurocode 4 (2005) were also programmed in the model. For brevity, the details of developing the utilized material models are not covered in the current article.

To accurately model CFTs with non-compact and slender cross-sections, an effective stress-strain model for steel was incorporated in the fiber model. The effective stress-strain model developed by Lai et al. (2016) was programmed for steel. The model accounts for local buckling of steel faceplates in compression and strain hardening in tension. This model was modified for elevated temperatures. These modifications involved updating the stiffness, yield strength and post-buckling strength in compression as a function of temperature. The equations for temperature dependence of yield strength (σ_y) and Young's modulus (E_s) were taken as recommended by Poh (2001). The developed stress-strain-temperature curves for elevated temperatures for steel with a yield strength of 300 MPa are shown in Fig. 1.

Fiber-Model Validation and Benchmarking

Validation was carried out at both ambient and elevated temperatures for the fiber model. Validation at ambient temperature involved comparing the results obtained from the fiber model with the calculated capacity per Chapter I of AISC 360 (AISC, 2016). Fig. 2 shows the normalized load versus axial displacement plots for compact, non-compact and slender CFT sections for conventional and effective steel models. Results obtained using conventional (elastic-perfectly-plastic) and effective (Lai et al. 2016) steel models for compact, non-compact and slender CFT sections are shown in Fig. 2(a) and Fig. 2(b), respectively. The load is normalized against the predicted column capacity per AISC 360 (Chapter I). All the columns buckled close to the AISC 360 predicted critical load. Hence the capacity predicted by the fiber model (at ambient

temperature) had a good agreement with the capacity estimated per AISC 360. Further, on comparing Fig. 2(a) and (b) it can be seen that effective stress-strain curves are more appropriate for non-compact and slender sections. For compact sections, the effective stress-strain model was seen to be over-conservative. This is because local buckling of steel faceplates before yielding is a concern only for non-compact/slender sections. Conventional (elastic-perfectly-plastic) stress-strain model gives better results for compact sections. The Eurocode models also do not consider local buckling and hence are recommended to be used only for compact sections.

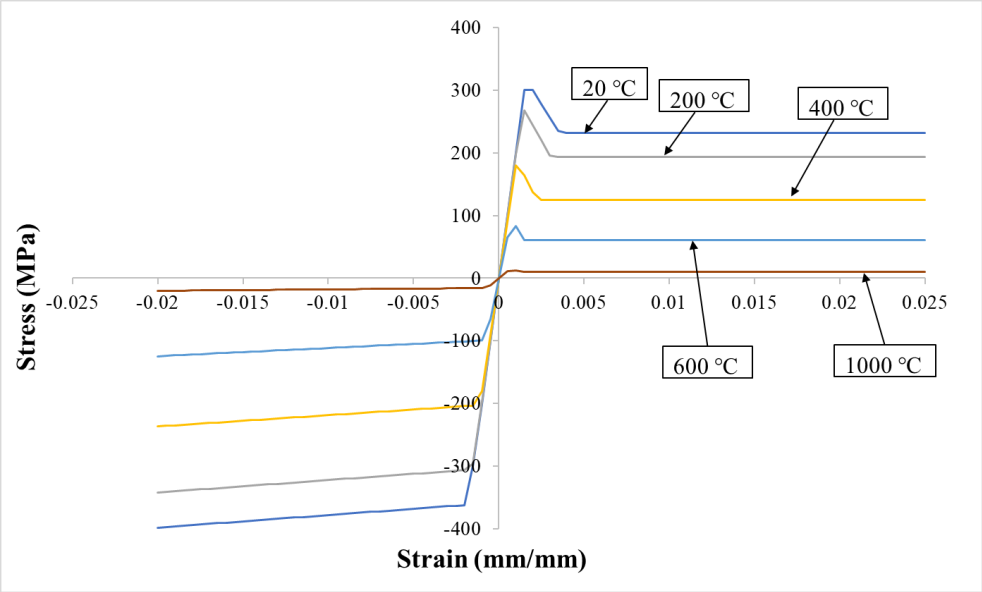

Figure 1: Modified effective stress-strain curves for 300 MPa steel at elevated temperatures for the steel model (Lai et al. 2016)

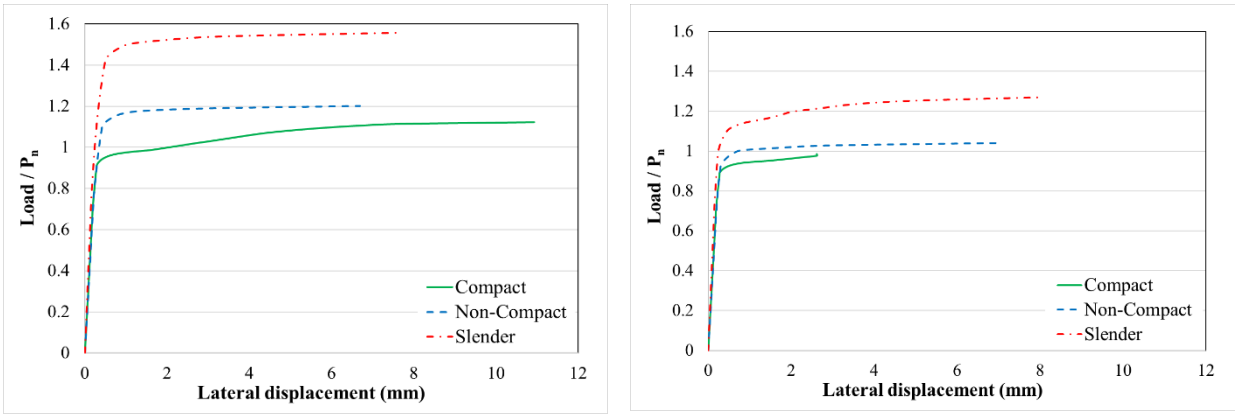

(a) (b)

Figure 2: Comparison of compressive strength (load vs. displacement) for (a) conventional (elastic-perfectly-plastic) and (b) effective (Lai et al. 2016) steel models versus AISC 360 predicted strength

Fiber model validation at elevated temperature was done by comparing results from the fiber model with FE models benchmarked by Bhardwaj et al. (2019b). Temperature profiles across the section of C-PSWs were compared with results obtained from FE analysis. The axial displacement

of different C-PSW models predicted by the fiber model was compared with FE models' results. Fig. 3 shows the comparison of temperature profile through the thickness of a 200 mm thick wall at two time instants obtained from FEM analysis and the fiber model. Fig. 4 presents the axial displacement predicted by FEM and the fiber model for three C-PSW models with wall thickness 200 mm and different slenderness. It can be seen that there is a good agreement in the results obtained from the fiber model and FE analysis

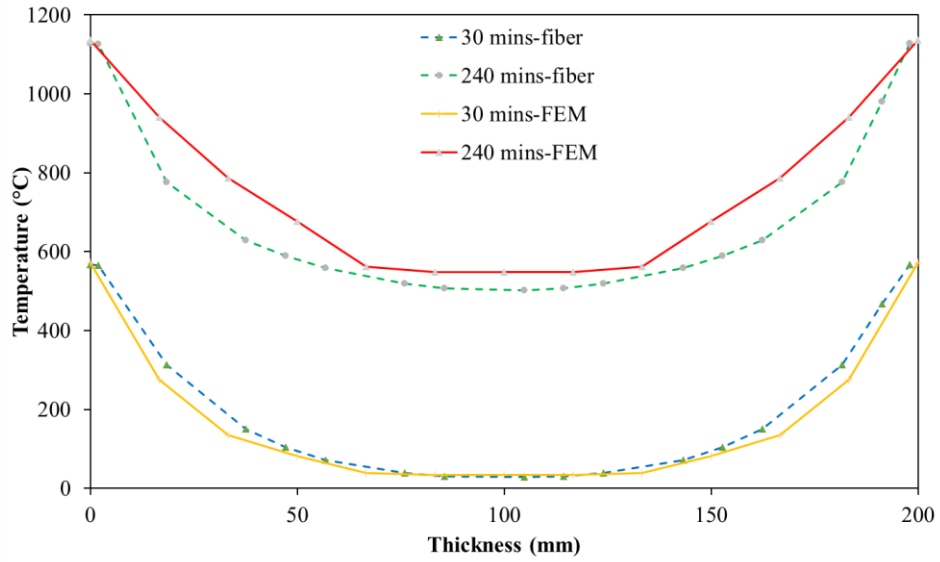

Figure 3: Temperature profiles across the section at various time instants: comparison of fiber model predicted and FEM data

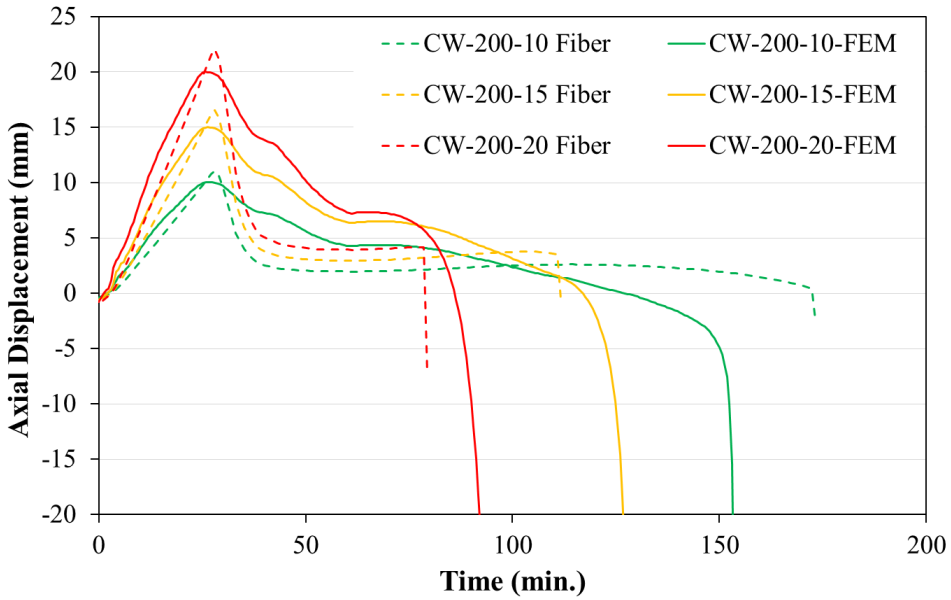

Figure 4: Comparison of axial displacement as predicted by fiber model and FE model for three C-PSW specimens

4. Parametric Studies and Capacity Prediction

The fiber model was utilized to perform a parametric study on CFT columns. The goal of this study was to understand how different parameters influence the CFT behavior, and to develop an

equation for capacity prediction. In all the cases a constant axial load was applied while the column surface was subjected to uniform elevated temperatures following the ASTM E119 standard time-temperature curve. Four parameters were considered in the parametric study namely aspect ratio of the column (ratio of width to depth), reinforcement ratio/section slenderness (steel faceplate thickness), steel yield strength, and concrete compressive strength. For each case, the analysis was performed for a range of column slenderness and axial load ratios. CFT models with column slenderness of 5, 10, 15, 20, 30, and 50 were studied. The axial load was increased from 10% to 100% of ambient nominal capacity in increments of 10%. The nominal axial capacity of CFTs was calculated per AISC 360, Chapter I. All the cases were studied without fire protection. The analytical study matrix is presented in Table 1. The nomenclature of the models presents the properties of the models in the order of aspect ratio, section slenderness, steel yield strength and concrete compressive strength.

Table 1: Parametric studies matrix for CFTs at elevated temperature

Nomenclature	Cross Section Dimensions (mm x mm)	Aspect Ratio	Steel Tube Thickness (mm)	Cross Section Slenderness	Steel Yield Strength-F_y (MPa)	Concrete Compressive Strength-f'_c (MPa)
C-1.0-50-358-38	300 x 300	1	6	50	358	38
C-1.5-50-358-38	250 x 360	1.5	7.2	50	358	38
C-2.0-50-358-38	210 x 420	2	8.4	50	358	38
C-1.0-33-358-38	300 x 300	1	9	33	358	38
C-1.0-50-358-38	300 x 300	1	6	50	358	38
C-1.0-66-358-38	300 x 300	1	4.5	66	358	38
C-1.0-100-358-38	300 x 300	1	3	100	358	38
C-1.0-50-358-38	300 x 300	1	6	50	358	38
C-1.0-50-413-38	300 x 300	1	6	50	413	38
C-1.0-50-482-38	300 x 300	1	6	50	482	38
C-1.0-50-358-27	300 x 300	1	6	50	358	27
C-1.0-50-358-38	300 x 300	1	6	50	358	38
C-1.0-50-358-48	300 x 300	1	6	50	358	48

Section Aspect Ratio

The column aspect ratio (ratio of column depth to width) was studied as a variable parameter. The cases were taken such that aspect ratio increased from 1 (C-1.0-50-358-38) to 2 (C-2.0-50-358-38) while section area and section slenderness remained nearly constant. The obtained critical load against slenderness plot at two surface temperatures is shown in Fig. 5. In the figure, the curves are plotted for two surface temperatures: 400 °C and 900 °C and the curves are identified by their aspect ratio in the legend. The aspect ratio does not have a very significant effect on column capacity at 400 °C and 900 °C (Fig. 5). While the column capacity increased slightly going from a ratio of 1 to 1.5 (for both 400 °C and 900 °C), it dropped again when the aspect ratio was further increased to 2. This is because as the depth of the column decreases (increasing aspect ratio), both moment of inertia ($I = bd^3/12$) and length ($L = slenderness\ x\ d$) reduce for a given column slenderness. As critical buckling load is a function of the ratio of effective stiffness to length, it is not affected significantly. However, the critical load reduces significantly with an increase in the surface temperature (Fig. 5).

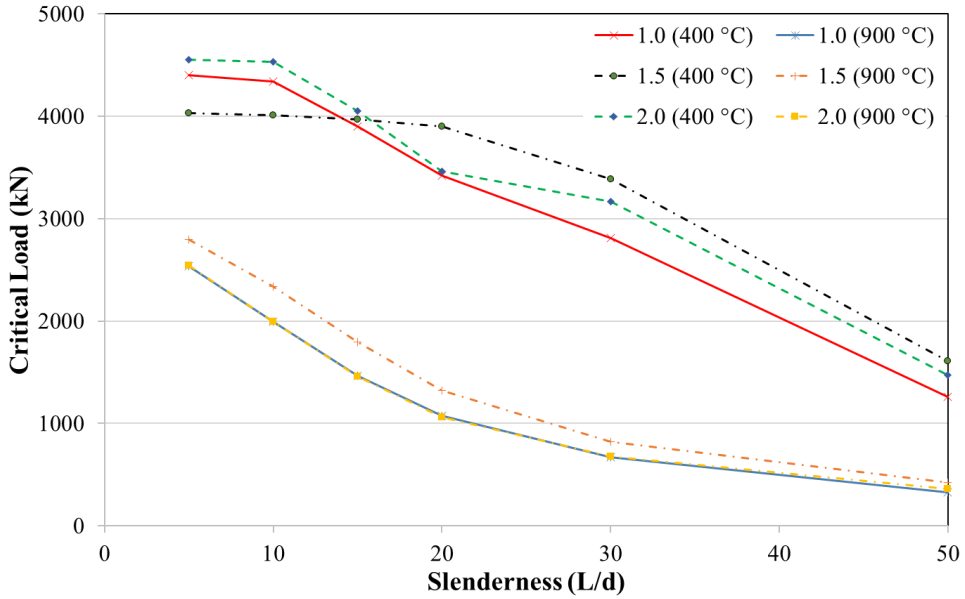

Figure 5: Critical load versus slenderness at two surface temperatures for various aspect ratios

Cross Section Slenderness

A range of section slenderness was considered by varying the thickness of steel faceplates while keeping the overall dimensions constant. The effective stress-strain model for steel was used for non-compact and slender sections, to account for local buckling of steel. The obtained critical load against slenderness plots are shown in Fig. 6, which has plots for 400 °C and 900 °C with the curves identified by section slenderness and temperature in the legend. Section slenderness has a significant effect on the critical load. The critical load decreased by nearly 40% for a non-compact section compared to a compact section. This is because local buckling for non-compact and slender sections prevents the steel from achieving its full yield strength. Thus, the column failed at lower axial loads. However, the effect of section slenderness decreases with increasing surface temperature, as the plots for 900°C are nearly coinciding. This is because steel resists lower fraction of the axial loads at higher temperatures, minimizing the effect of local buckling on overall capacity.

Steel Yield Strength

Steel yield strength was ranged from 358 MPa to 482 MPa to study its effect on column behavior. The results from these models are shown in Fig. 7, the plots identified by steel yield strength and temperature in the legend. The figure shows that steel yield strength does not significantly affect the load capacity of CFTs. The capacity of columns increased slightly at 400°C by increasing steel strength. However, the effect of steel yield strength was negligible at 900°C and the results were close. This occurred due to strength degradation of steel at high temperatures, which resulted in concrete resisting most of the applied axial load.

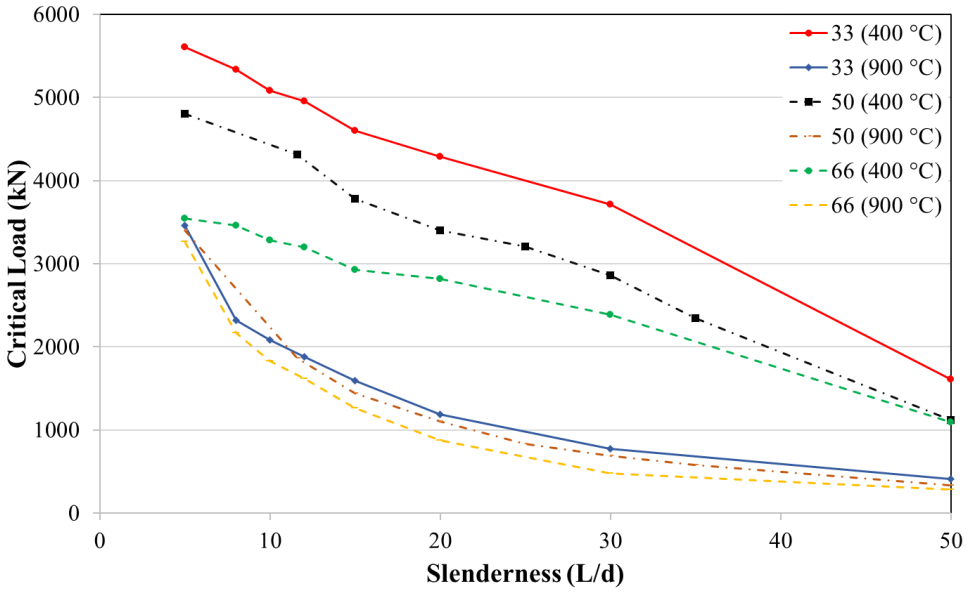

Figure 6: Critical load versus slenderness versus temperature curves for varying section slenderness (reinforcement ratio)

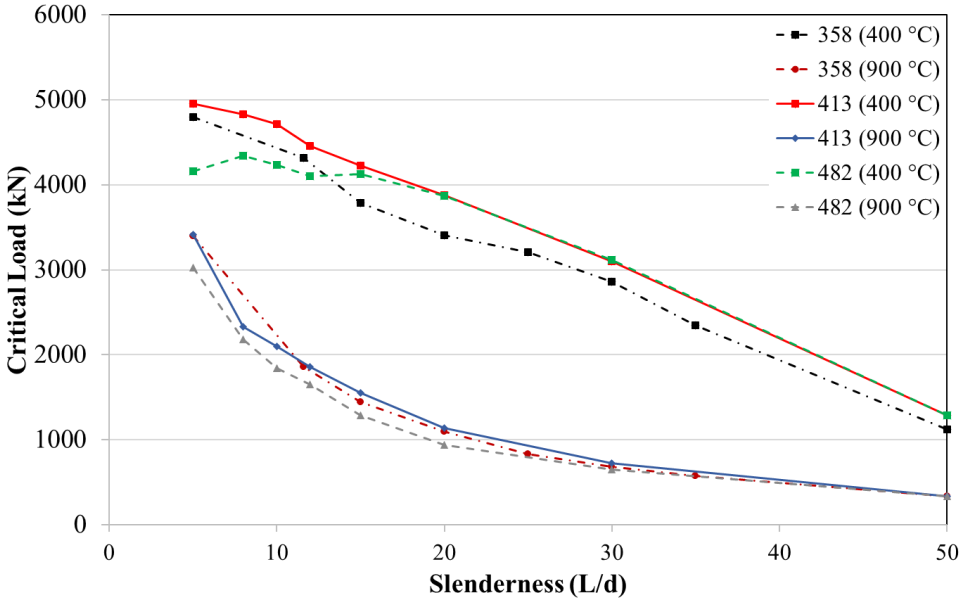

Figure 7: Critical load versus slenderness versus temperature curves for varying steel yield strength

Concrete Compressive Strength

Concrete compressive strength (f'_c) was varied from 27 MPa to 48 MPa, to study its effect on column capacity. The obtained results are compared in Fig. 8. The plots are identified by concrete compressive strength and surface temperature in the legend. Fig. 8 shows that the load capacity of CFTs increases with increasing concrete compressive strength for a surface temperature of 400 °C. However, the capacity shows a smaller increase when the surface temperature is 900 °C. Concrete compressive strength has a significant influence on the CFT capacity as most of the concrete remains at relatively low temperatures due to its low thermal conductivity. At elevated

temperatures, concrete carries most of the applied axial load and changing its strength affects column capacity.

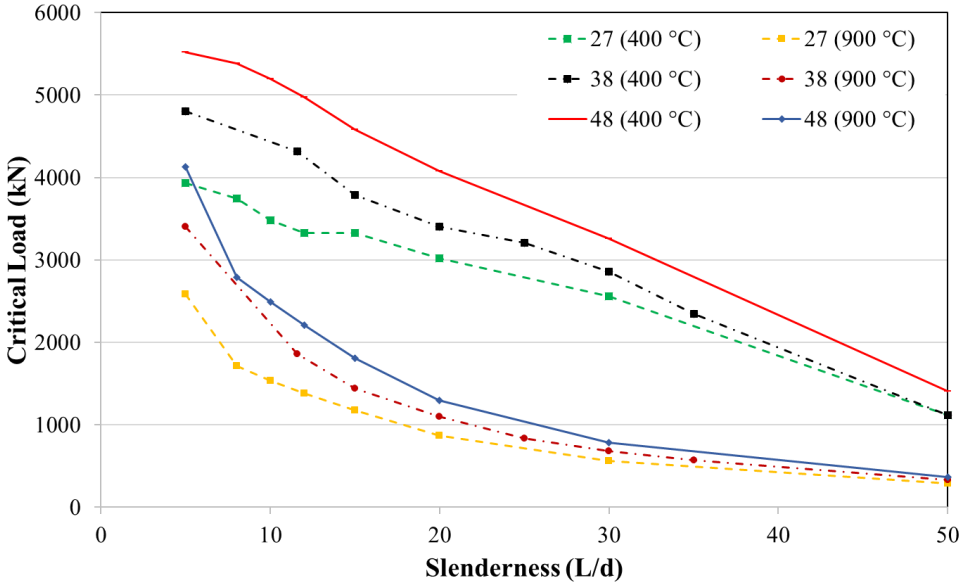

Figure 8: Critical load versus slenderness versus temperature curves for varying concrete compressive strength

Capacity Prediction Equation for CFTs at Elevated Temperature

Based on the results of the parametric study, a set of equations to predict the capacity of CFTs at elevated temperatures was proposed. For this purpose, the results from the parametric studies were normalized to be plotted on a single graph. The experimental critical load [$P_{cr}(T)$], the axial load applied on the CFT column for each iteration, was normalized to the calculated nominal axial compressive strength (zero length) of the column at the failure time [$P_{no}(T)$]. This nominal capacity was calculated based on the steel surface temperature and the temperature of all the concrete elements (at failure). This non-dimensional ratio [$P_n(T)/ P_{no}(T)$] was plotted on the y-axis. The equations used for its calculation are given below:

For compact sections ($\lambda < \lambda_p$),

$$P_{no}(T) = A_s F_y(T) + 0.85 \sum_{i=conc\_elements} f'_c(T_i) A_{ci} \tag{1}$$

For non-compact sections ($\lambda_p < \lambda < \lambda_r$),

$$P_{no}(T) = P_p - \frac{P_p - P_y}{\lambda_r - \lambda_p}\left(\lambda - \lambda_p\right)^2 \tag{2}$$

$$\text{where } P_p(T) = A_s F_y(T) + 0.7 \sum_{i=conc\_elements} f'_c(T_i) A_{ci} \tag{2a}$$

For slender sections ($\lambda > \lambda_r$),

$$P_{no}(T) = A_s F_{cr}(T) + 0.7 \sum_{i=conc\_elements} f'_c(T_i) A_{ci} \tag{3}$$

$$\text{where } F_{cr}(T) = \frac{9E_s(T)}{\left(\frac{b}{t_s}\right)^2} \tag{3a}$$

In these equations, slenderness ratio (λ) is defined as (b/t_s) where b and t_s are the larger column dimension and steel faceplate thickness, respectively. A_s is the cross-sectional area of steel faceplates and $F_y(T)$ is the yield strength of steel at failure surface temperature. For concrete, summation was carried out over all concrete elements where $f'_c(T)$ is the compressive strength for the given element temperature and A_{ci} is the area of that element. Steel and concrete strengths as a function of temperature were calculated from Tables A-4.2.1 and A-4.2.2 of AISC 360. This normalized critical load is plotted against the ratio of [$P_{no}(T)$] to elastic buckling strength [$P_e(T)$] at the failure temperature [$P_{no}(T)/P_e(T)$] on the x-axis. The elastic buckling capacity at failure temperature is calculated as follows:

$$P_e(T) = \frac{\pi^2 EI_{eff}(T)}{(L_c)^2} \tag{4}$$

$$(EI)_{eff} = E_s(T)I_s + C_3 \sum_{i=conc\_elements} E_c(T_i)I_{ci} \tag{5}$$

$$C_3 = 0.45 + 3\left(\frac{A_s}{A_g}\right) \leq 0.9 \tag{6}$$

Where A_s is the area of steel faceplates and A_g is the gross section area. $EI_{eff}(T)$ is the effective section stiffness, which is calculated using Eq. 5. L_c is the effective length of the column, which depends on the boundary conditions. $E_s(T)$ is the steel modulus of elasticity at failure surface temperature, and $E_c(T_i)$ is the modulus of elasticity of concrete elements based on the associated temperature at failure. I_s and I_c are the moments of inertia of steel and concrete sections respectively, calculated about the centroid of the section. C_3 is the concrete contribution factor to stiffness, which is calculated as given in Eq. 6. Based on the data points obtained from fiber analysis, curve-fitting was done to obtain a lower-bound curve, a median curve and a simplified bi-linear curve. These equations are given below:

Lower bound:

$$P_{cr}(T) = P_{no}(T)\left[0.54^{\left(\frac{P_{no}(T)}{P_e(T)}\right)^{0.3}}\right] \tag{7}$$

Median:

$$P_{cr}(T) = P_{no}(T)\left[0.80^{\left(\frac{P_{no}(T)}{P_e(T)}\right)^{0.8}}\right] \tag{8}$$

Simplified bi-linear:

$$P_{cr}(T) = P_{no}(T)\left[1 - 0.4\left(\frac{P_{no}(T)}{P_e(T)}\right)\right] \text{ if } \frac{P_{no}(T)}{P_e(T)} < 1 \tag{9a}$$

$$P_{cr}(T) = 0.06P_{no}(T)\left[11 - \frac{P_{no}(T)}{P_e(T)}\right] \text{ if } \frac{P_{no}(T)}{P_e(T)} \geq 1 \tag{9b}$$

Where $P_{no}(T)$ is the nominal axial compressive strength (zero length) of the column at failure time, calculated as given in Eq. 1 to 3. $P_e(T)$ is the elastic buckling strength of the column at failure time, which is calculated using Eq. 4. Fig. 9 plots all the normalized fiber model results (data points), and the proposed design equations.

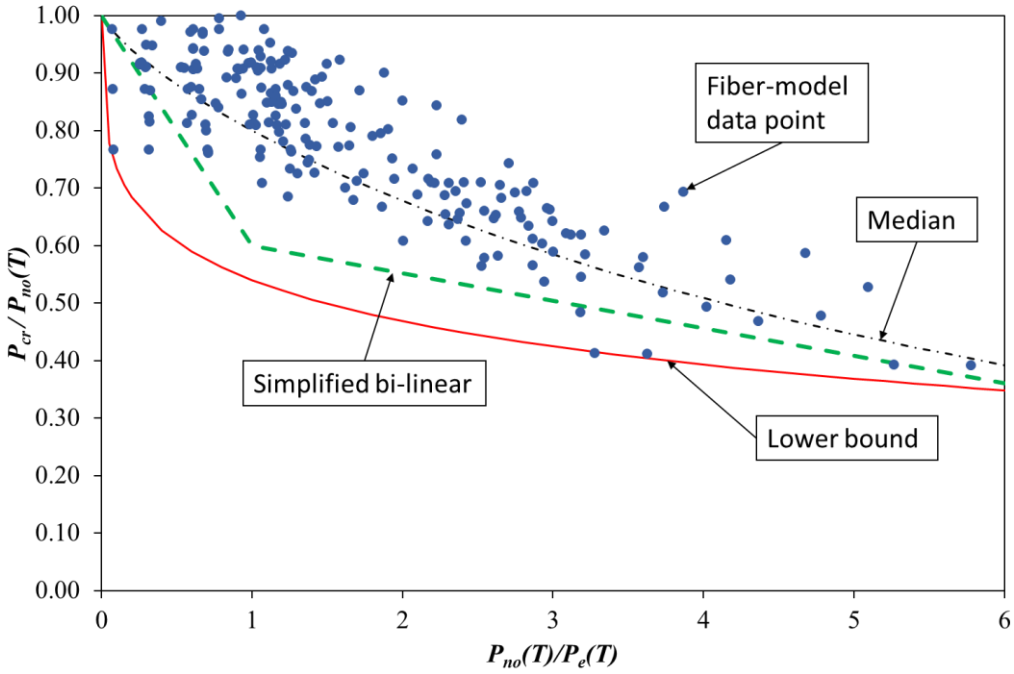

Figure 9: Normalized results of the parametric studies plotted with the proposed theoretical capacity curves (lower-bound, median and simplified bi-linear)

The lower-bound curve is significantly conservative in predicting CFT capacity comparing to the fiber model results as shown in Fig. 9. This equation can be used to estimate the axial load capacity of CFTs, given its properties and the targeted fire resistance rating. A 2D heat transfer needs to be conducted up to the required time (fire rating) to obtain the temperature distribution through the cross-section (1D heat transfer may suffice for some cases, e.g., square columns subjected to uniform fire). Based on the steel and concrete temperatures obtained, $P_{no}(T)$ and $P_e(T)$ can be calculated. The lower bound critical load can then be obtained using Eq. 7.

5. Summary and Conclusions

This paper presents a study of strength and stability behavior of CFT columns at elevated temperatures. For this purpose, a cross-section based 2D fiber model was developed to simulate composite axial members under fire loading. The fiber model was validated at ambient and elevated temperatures using experimental data and 3D FE results. Using this fiber model, the effects of various parameters on the stability of CFTs at elevated temperatures were investigated. A capacity equation for CFTs at elevated temperatures was also developed and proposed.

Results of the parametric study indicated that concrete compressive strength and section slenderness have a significant influence on the capacity of CFTs. Load capacity of CFTs was seen to decrease with decreasing concrete strength and increasing cross section slenderness. However, steel yield strength and aspect ratio had a minor effect of the load capacity. Also, it was observed that column capacity was nearly independent of all the four parameters at high temperatures (~900°C). Design equations were proposed to calculate the capacity of CFTs at elevated temperatures. A lower bound, a median, and a simplified bi-linear equation were proposed based on the parametric study results. The limiting assumptions made in the development of the fiber

model can be further minimized through additional research and development, which would expand the scope of applicability of the model. A study to develop equations for predicting fire resistance (time-to-failure) of composite axial members is planned in future.

Acknowledgments

The project is funded by Charles Pankow Foundation, Steel Institute of New York (SINY), and American Institute of Steel Construction (AISC). The authors are grateful to these agencies for financial support. The authors also acknowledge the technical inputs received from the advisory panel.

References

AISC (American Institute of Steel Construction). (2016). "Specification for Structural Steel Buildings", 15th Edition, AISC 360, Chicago, IL

ASTM (American Standards of Testing and Materials). (2000). "Standard Test Methods for Fire Tests of Building Construction and Materials", ASTM E119, West Conshohocken, PA

Bhardwaj, S.R., Varma, A.H., and Wazalwar, P. (2019a). "Axial Force-Biaxial Moment-Vector Shear (P-M-V) Interaction for Steel-Plate Composite (SC) Wall Piers." *Nuclear Engineering and Design* 349 (April): 162–73. https://doi.org/10.1016/j.nucengdes.2019.04.022.

Bhardwaj, S., Sharma, S., & Anvari, A. T., Varma, A. H (2019b). "On the stability of composite plate shear walls under fire loading." *Proceedings of the Annual Stability Conference-Structural Stability Research Council*, St. Louis, MO, April 2-5, 2019

Eurocode 4. (2005). "Design of composite steel and concrete structures- Part 1-2: General rules - Structural fire design"

Hong, S. (2007). "Fundamental Behavior and Stability of CFT Columns Under Fire Loading", Purdue University

Hong, S., Varma, A. H. (2008). "Analytical modeling of the standard fire behavior of loaded CFT columns", Journal of Constructional Steel Research

Hong, S., Varma, A. H. (2009). "Predicting Fire Behavior of Composite CFT Columns Using Fundamental Section Behavior", Journal of ASTM International, Vol. 7, No. 1

Kodur, V. K. R.; Mackinnon, D. H. (2000). "Design of Concrete-Filled Hollow Structural Steel Columns for Fire Endurance." Engineering Journal - American Institute of Steel Construction 37 (1): 13–24.

Lai, Z., Varma, A. H. (2016). "Effective Stress-Strain Relationships for Analysis of Non-compact and Slender Filled Composite (CFT) Members", Engineering Structures

Lie, T., ed. (1992). "Structural Fire Protection" Manual and Reports on Engineering Practice No. 78, ASCE, New York, N.Y.

Lie, T. T. and Irwin, R. J. (1995). "Fire Resistance of Rectangular Steel Columns Filled with Bar-Reinforced Concrete," *J. Struct. Eng.*, Vol. 121, No. 5, 1995, pp. 797–805.

Lue, Dung, M. (2006). "Experimental study on rectangular CFT columns with high-strength concrete", Journal of Constructional Steel Research 63 (2007) 37–44

MathWorks (2019). *MATLAB R2019b Documentation*, The MathWorks Inc., Natick, MA

Poh, K. W. (2001). "Stress-Strain-Temperature Relationship for Structural Steel", Journal of Materials in Civil Engineering. Vol. 13 pp 371-379

Simulia (2016). *ABAQUS 2017 Documentation*, Dassault Systemes Simulia Corporation Providence, RI